materials

MDPI

Article

Influence of Li_2Sb Additions on Microstructure and Mechanical Properties of Al-20Mg_2Si Alloy

Hong-Chen Yu, Hui-Yuan Wang *, Lei Chen, Min Zha *, Cheng Wang, Chao Li and Qi-Chuan Jiang

Key Laboratory of Automobile Materials of Ministry of Education & School of Materials Science and Engineering, Nanling Campus, Jilin University, No. 5988 Renmin Street, Changchun 130025, China; hcyu14@mails.jlu.edu.cn (H.-C.Y.); DanLuo198709@gmai.com (L.C.); chengwang@jlu.edu.cn (C.W.); chaoli14hcyu14@mails.jlu.edu.cn (C.L.); jqc@jlu.edu.cn (Q.-C.J.)

* Correspondence: wanghuiyuan@jlu.edu.cn (H.-Y.W.); minzha@jlu.edu.cn (M.Z.); Tel.: +86-431-8509-4699 (H.-Y.W. & M.Z.)

Academic Editor: Daolun Chen

Received: 9 February 2016; Accepted: 21 March 2016; Published: 29 March 2016

Abstract: It is found that Li_2Sb compound can act as the nucleus of primary Mg_2Si during solidification, by which the particle size of primary Mg_2Si decreased from ~300 to ~15–25 μm. Owing to the synergistic effect of the Li_2Sb nucleus and adsorption-poisoning of Li atoms, the effect of complex modification of Li-Sb on primary Mg_2Si was better than that of single modification of Li or Sb. When Li-Sb content increased from 0 to 0.2 and further to 0.5 wt.%, coarse dendrite changed to defective truncated octahedron and finally to perfect truncated octahedral shape. With the addition of Li and Sb, ultimate compression strength (UCS) of Al-20Mg_2Si alloys increased from ~283 to ~341 MPa and the yield strength (YS) at 0.2% offset increased from ~112 to ~179 MPa while almost no change was seen in the uniform elongation. Our study offers a simple method to control the morphology and size of primary Mg_2Si, which will inspire developing new Al-Mg-Si alloys with improved mechanical properties.

Keywords: Al-Mg-Si alloy; mechanical properties; heterogeneous nucleation; primary Mg_2Si

1. Introduction

The as-cast microstructure has a strong influence on mechanical properties of castings [1]. For Al-high Mg_2Si alloy, the formation of primary Mg_2Si reinforcement with small grain size and regular morphology is necessary to improve the mechanical properties of alloys and thus is has become the main issue when preparing the materials with excellent properties [2–5]. Intermetallic compound Mg_2Si, which exhibits low density (1.99×10^3 kg m^{-3}), high melting temperature (1085 °C), high elastic modulus (120 GPa) and high hardness (4.5×10^9 N m^{-2}) as well as a low thermal expansion coefficient (TEC) (7.5×10^{-6} K^{-1}), has been widely used as a reinforced phase to prepare Al/Mg_2Si alloys [6–9]. The excellent properties of Mg_2Si can make Al/Mg_2Si alloys suitable for widespread use in automobile and aerospace fields [10–13]. However, under equilibrium solidification condition, primary Mg_2Si tends to form coarse dendrite, which is harmful to the mechanical property of Al-Mg_2Si alloys and limits their development and application [14–16]. Therefore, controlling the morphology and size of primary Mg_2Si is a great challenge to material scientists [17].

As far as we know, modification treatment is the most effective method to control morphologies and sizes of primary and eutectic Mg_2Si, which is readily available for commercial applications [18]. Among all kinds of modifiers, Sb has been widely used for modification treatment of primary and eutectic Mg_2Si [19,20]. The reason is that Mg_3Sb_2 formed during solidification can act as the nucleus of primary and eutectic Mg_2Si, refining the size of Mg_2Si and improving mechanical properties of

Al-Mg-Si alloys [19,20]. Alizadeh *et al.* [21] reported that with the addition of 0.2 wt.% Sb into the Mg-4Zn-2Si melt, flake-like eutectic Mg_2Si changed into fine polygons, and the mechanical properties such as impression creep and hot hardness were improved significantly. In our previous study [22], we found that with the content of Sb addition increasing from 0 to 0.2 and to 0.5 and finally to 2 wt.%, the morphology of primary Mg_2Si in Mg-4Si, alloys transformed from coarse dendrite to equiaxed-dendrite and to defective octahedron and finally to perfect octahedron; meanwhile, the morphology of eutectic Mg_2Si transformed from flake-like to fine polygonal shapes. Based on the above research, one can see that the modification effect of Sb is more effective to eutectic Mg_2Si than to primary Mg_2Si. Therefore, how to enhance the modification effect of Sb on primary Mg_2Si is the key to improving mechanical properties of Al-high Mg_2Si alloy. However, only limited research has been reported regarding this issue.

Because the electronegativity difference between Li and Sb is relatively large, they could form compounds with thermodynamic stability such as Li_2Sb and Li_3Sb during solidification process. The calculated disregistry is 4.0% at the orientation relationship of $(10\bar{1}0)_{Li_2Sb}//(111)_{Mg_2Si}$ for Li_2Sb while 5.8% at that of $(001)_{Li_3Sb}//(001)_{Mg_2Si}$ for Li_3Sb, which are both less than 6.0% and may act as the nucleation substrate for primary Mg_2Si [23]. To change morphologies and refine the size of primary Mg_2Si during solidification and finally to improve the mechanical properties of Al-20Mg_2Si alloy, we added Li and Sb simultaneously to the Al-Mg-Si melt. The mechanism of primary Mg_2Si co-modified with Li and Sb was revealed in this research. The compression property and microhardness of Al-20Mg_2Si alloys modified with 0, 0.2 and 0.5 wt.% Li-Sb were also tested. The results achieved will be a big step forward in realizing the artificial manipulation of grain refinement and morphology transformation of primary Mg_2Si in Al alloys, which plays an important role in improving physical and mechanical properties of Al-Mg-Si alloys.

2. Experimental Section

2.1. Preparation of Al-20Mg_2Si Alloy Modified with Various Contents of Li-Sb

In order to prepare Al-20Mg_2Si alloy, where the unit of "20" is "wt.%" and the unit of "2" is the number of Mg atom in intermetallic compound Mg_2Si, the contents of the Al ingot (99.98 wt.% purity), Mg ingot (99.85 wt.% purity) and Al-24.4Si master alloy are ~57.2 wt.%, ~12.6 wt.% and ~30 wt.%, respectively. The modifiers are pure Sb ingot (98.00 wt.% purity) and Mg-13.5Li master alloy. Pure Al and Al-24.4Si master alloy were melted at 750 °C in a graphite crucible in an electric resistance furnace of 5 kW; then pure Mg, Sb and Mg-13.5Li master alloy preheated at 150 °C in a vacuum oven were added to the melts together. The designed compositions of Li-Sb in melts were 0, 0.2 and 0.5 wt.%, with an atomic ratio of Li:Sb of 3:1. Manual agitation was conducted in the Al-Mg-Si melts for about 1 min and held at 750 °C for 20 min. Finally, the melts was poured into a steel mold preheated at 150 °C to produce Al-20Mg_2Si alloy co-modified with various contents of Li and Sb.

2.2. Characterization

Metallographic samples with a size of 10 mm × 10 mm × 13 mm were cut at the bottom of the ingots. Metallographic samples were prepared by a standard procedure and etched with 0.5 vol.% HF-distilled water solution for about 30 s at room temperature. To observe the 3-D morphologies of primary Mg_2Si, samples with the size of 1.2 mm × 12 mm × 13 mm were put into a 20 vol.% HNO_3-distilled water solution to dissolve the Al covering on the surface of the primary Mg_2Si. The samples for compression test were processed into cylinders of which the diameter is 3 mm and the height is 6 mm. X-ray diffraction (XRD) (D/Max 2500PC, Rigaku, Tokyo, Japan) was used to characterize phase constitutions of the samples, using CuK_α radiation in step modes from 20° to 80° with a scanning speed of 4° min^{-1} and an acquisition step of 0.02° (2θ). As-cast microstructures of Al-20Mg_2Si alloy were investigated using optical microscopy (OM) (Carl Zeiss-Axio Imager A2m, Gottingen, Germany). The 3-D morphologies of the extracted primary Mg_2Si were observed using a

field emission scanning electron microscope (FESEM) (JEOL-6700F, JEOL, Tokyo, Japan). A scanning electron microscope (SEM) (EVO 18, Carl Zeiss, Mainz, Germany) equipped with an energy dispersive spectrometer analyzer (EDS) was used to observe the elemental surface scanning spectra. The nucleus of primary Mg_2Si was explored by transmission electron microscopy (TEM) (JEM-2100, JEOL, Tokyo, Japan) equipped with an EDS analyzer (EDS6498, OXFORD, London, Britain) under an operating voltage of 200 kV. The compression tests of Al-20Mg_2Si alloy were conducted in a MTS (INSTRON-5869, INSTRON, Boston, MA, USA) machine operating with a constant crosshead speed of height × 0.018 mm/min at room temperature. At least three compression tests were done for each condition to ensure the accuracy of results. The microhardness of Al matrix in Al-20Mg_2Si alloy were tested by Microhardness Tester (1600-5122VD Micromet 5104, Buehler, Chicago, IL, USA), and at least seven measurements were done for each condition to ensure the accuracy of the results.

3. Results and Discussion

3.1. Microstructure of Al-20Mg_2Si Alloy Modified with Li and Sb Simultaneously

According to the XRD results (Figure 1a–c), only Al and Mg_2Si phases were found in the alloy. No characteristic peaks of compounds containing Li or Sb were detected in the modified alloys, which should be because the content of Li and Sb addition is limited. As-cast microstructures of Al-20Mg_2Si alloys with 0, 0.2 and 0.5 wt.% Li-Sb additions are given in Figure 2a–f. With the addition of Li and Sb, the size of primary Mg_2Si (see black arrows in Figure 2a–c) (Figure 2a) decreased from ~300 to ~15–25 μm and their morphologies changed into polyhedron (Figure 2b,c); the sizes of eutectic Mg_2Si (see black arrows in Figure 2d–f) in modified alloys are also refined significantly despite the 2-D morphologies of eutectic Mg_2Si still remaining flake-like (Figure 2d–f). Interestingly, one can see some dark spots occasionally located in the center of the polygons (see white arrows), which should be the nucleus of primary Mg_2Si (Figure 2b,c).

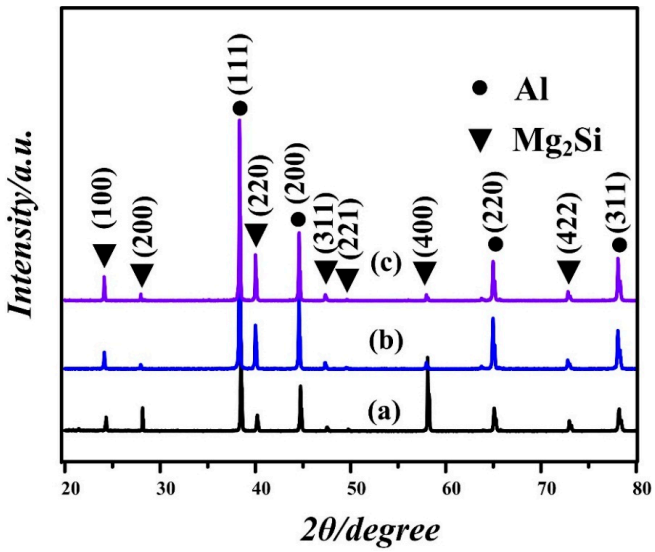

Figure 1. XRD patterns for Al-20Mg_2Si alloy without and with various Li and Sb contents: (**a**) 0; (**b**) 0.2; and (**c**) 0.5 wt.% Li-Sb.

According to the literature [22,24], Li or Sb can restrict the growth of Mg_2Si crystal by adsorbing on the growth sites of primary Mg_2Si particles, and hence refine their size. For comparison, 0.2 wt.% Li and 0.2 wt.% Sb were separately added to Al-20Mg_2Si alloys. As-cast microstructure of primary Mg_2Si modified with 0.2 wt.% Li or Sb is shown in Figure 3a,b, respectively. Clearly, the grain refinement effect of 0.2 wt.% Li or Sb is relatively weaker than that of the combined addition of 0.2 wt.% Li-Sb (Figure 3c). Moreover, the 3-D morphologies of primary Mg_2Si modified with 0.2 wt.% Li or Sb are

also given (Figure 3d–g). As we can see, perfect octahedrons and equiaxed-dendrites were obtained in Al-20Mg_2Si alloy modified with 0.2 wt.% Li (Figure 3d,e). Similar morphologies were also observed in the alloy modified with 0.2 wt.% Sb (Figure 3f,g). Meanwhile, truncated octahedral primary Mg_2Si was formed when modified with 0.2 wt.% Li-Sb (Figure 3h). Apparently, compared with the modification effect of Li or Sb on primary Mg_2Si, the co-modification effect of Li-Sb was enhanced significantly.

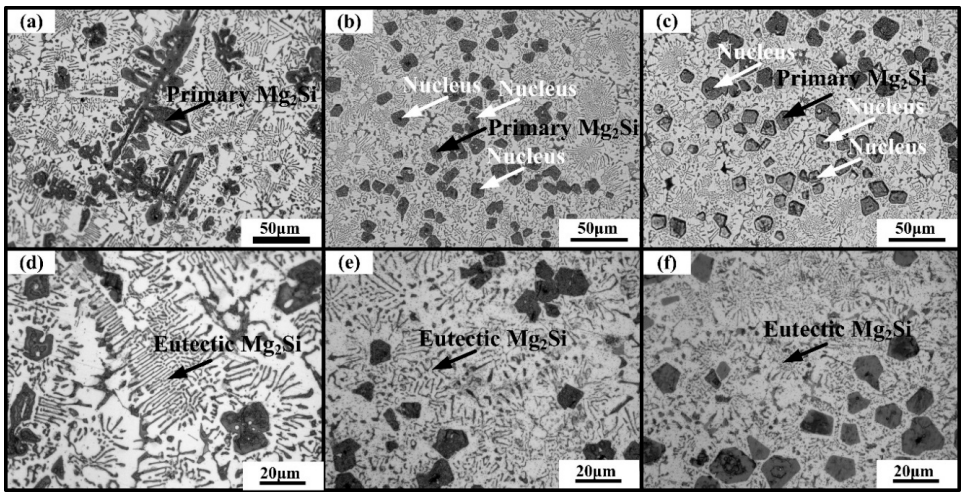

Figure 2. Microstructures of as-cast Al–20Mg_2Si alloys without and with various Li-Sb contents: primary Mg_2Si in (**a**) 0; (**b**) 0.2; and (**c**) 0.5 wt.% Li-Sb; eutectic Mg_2Si in (**d**) 0; (**e**) 0.2; and (**f**) 0.5 wt.% Li-Sb.

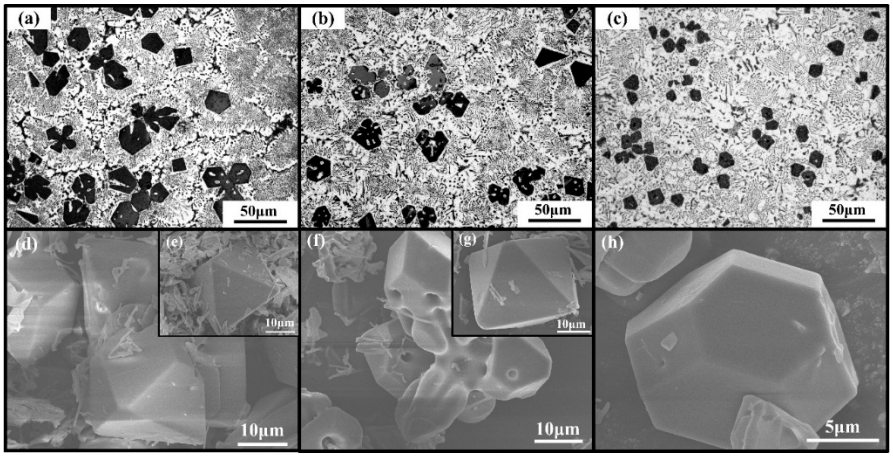

Figure 3. Microstructure images of primary Mg_2Si in as-cast Al–20Mg_2Si alloys modified with: (**a**) 0.2 wt.% Li; (**b**) 0.2 wt.% Sb; and (**c**) 0.2 wt.% Li-Sb. FESEM images of primary Mg_2Si extracted from Al–20Mg_2Si alloys modified with: (**d**–**e**) 0.2wt.% Li; (**f**–**g**) 0.2 wt.% Sb; and (**h**) 0.2 wt.% Li-Sb.

3.2. Characterization of Nucleus in Primary Mg_2Si

To identify the composition of the nucleus, shown in Figure 1b,c, elemental mapping scanning analysis was conducted. Note that the distribution of Li was not given because Li is a light element, which is difficult to be detected by EDS. As we can see, the Al atoms were mostly around the primary Mg_2Si crystal (Figure 4b); Mg (Figure 4c) and Si (Figure 4d) atoms were detected in the crystal, while Sb atoms were mainly found inside the nucleus and the intensity of Sb (Figure 4e). Therefore, it is rational to say that the nucleus is a kind of antimony compound.

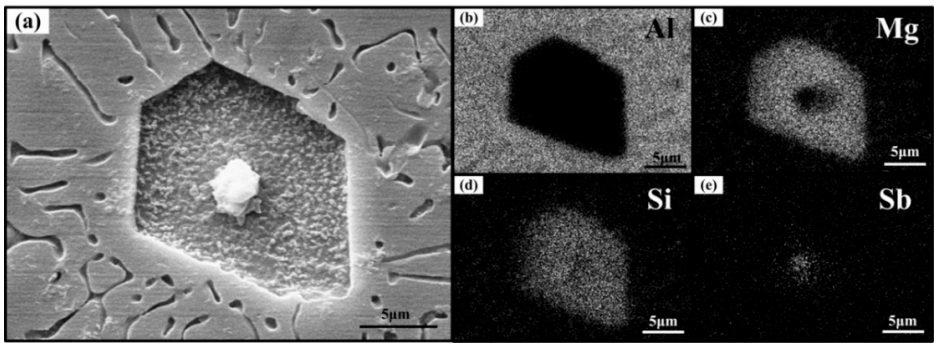

Figure 4. (**a**) The SEM micrograph and elemental surface scanning spectra for Al-20Mg_2Si alloys modified with Li-Sb for: (**b**) Al; (**c**) Mg; (**d**) Si; and (**e**) Sb.

Further investigation on the nature of nucleus was carried out by TEM and EDS. A nucleus located in the center of primary Mg_2Si co-modified with Li-Sb is shown in Figure 5a. According to the double selected-area diffraction (SAD) pattern of nucleus (Figure 5b), the antimony-containing compound is Li_2Sb, which has a hexagonal structure (P-62m) with the lattice constant of a = 0.7947 nm, b = 0.7947 nm, c = 0.3260 nm, $\alpha = \beta = 90^\circ$ and $\gamma = 120^\circ$ [23]. In our previous study, we have confirmed that the Si sites in Mg_2Si lattice can be substituted by Sb atoms when Sb was added into the Mg-4Si alloy [22], while no substitution occurred when Ca and Sb were simultaneously added to the Al-20Mg_2Si alloy [22,25]. To investigate whether substitution occurred in the present case, the EDS analysis for the modified Mg_2Si crystal and the nucleus is given in Figure 5c,d, respectively. According to the result, the EDS collected from the modified Mg_2Si crystal contains mainly Mg, Si and Al peaks; only a few (0.09 at.%) Sb atoms were detected in the Mg_2Si crystal (Figure 5c), while the EDS obtained from nucleus contains Mg, Sb (31.3 at.%), Si and Al peaks (Figure 5d). Thus, it can be concluded that most of the Sb atoms reacted with Li atoms to form Li_2Sb compounds, acting as nucleus for Mg_2Si crystals.

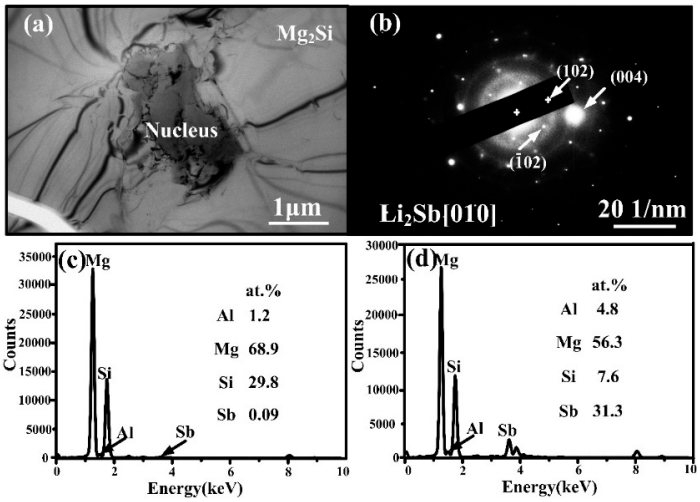

Figure 5. (**a**) TEM micrograph of the modified Mg_2Si crystal with a nucleus; (**b**) selected-area diffraction (SAD) pattern of the nucleus in (a); (**c**) EDS for the modified Mg_2Si crystal; and (**d**) EDS for the nucleus in (a), respectively.

Note that, in our experiment, the designed atomic ratio of Li:Sb is 3:1, while the nucleus is Li_2Sb, so that slight substitution of Sb atoms in Mg_2Si lattice may also occur. In general, with the growth of crystal, the crystal facets with high growth rates will shrink gradually, while the facets with low growth rates will be reserved as crystal surfaces [26]. This suggests that some Li atoms did not react

with Sb and they might be absorbed on the {100} facets. According to Figure 3a,d,e, sub-modification occurred in Al-20Mg_2Si alloy with 0.2 wt.% Li added. Therefore, as for the primary Mg_2Si modified with 0.2 wt.% Li-Sb, in addition to that Li_2Sb nucleus can promote the nucleation of primary Mg_2Si, additional Li atoms absorbed on {100} facets led to the exposure of {100} facets, and thus truncated octahedral primary Mg_2Si formed, as shown in Figure 3h.

3.3. Effect of Li_2Sb Nucleus on Mechanical Properties of Al-20Mg_2Si Alloy

The mechanical properties of Al-20Mg_2Si alloys with 0, 0.2 and 0.5 wt.% Li-Sb addition are given in Figure 6 and Table 1. With the addition of Li and Sb, ultimate compression strength (UCS) of Al-20Mg_2Si alloys increased from ~283 to ~341 MPa and the yield strength (YS) at 0.2% offset increased from ~112 to ~179 MPa, while almost no change was seen in the uniform elongation. The addition of Li and Sb also resulted in the increase in microhardness of α-Al matrix from ~91 to ~104 Hv. For a particle reinforced alloy, mechanical property is influenced by the reinforcement to a significant extent [10]. It is well known that primary Mg_2Si is the reinforced phase in Al-20Mg_2Si alloys and dendritic primary Mg_2Si with a large size is harmful to mechanical properties [14–16]. Decreasing particle size usually leads to an increase in strength according to the Hall-Petch effect: [10].

$$\Delta\sigma_{YS} \approx D^{-1/2}\left(\frac{V_m}{V_\gamma}\right)^{1/6}$$

where $\Delta\sigma_{YS}$ is the increment of yield strength; D is the size of reinforcement phase; and V_m and V_γ are the volume fraction of matrix and reinforcement, respectively. Thus, with the addition of Li-Sb, the size of primary Mg_2Si decreases from ~300 to ~15–25 μm (Figure 2a–c), leading to improved UCS, YS, and microhardness of Al-20Mg_2Si alloys.

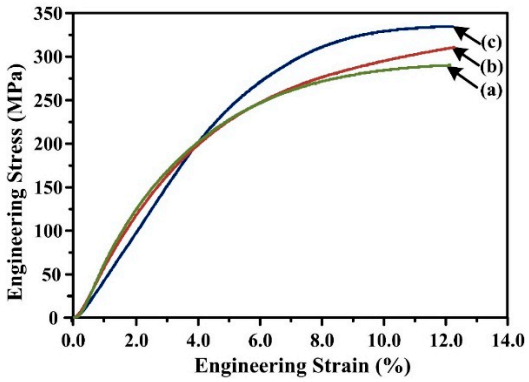

Figure 6. Engineering stress-stain curves of Al-20Mg_2Si alloys: with: (**a**) 0; (**b**) 0.2; and (**c**) 0.5 wt.% Li-Sb addition.

Table 1. Mechanical properties of Al-20Mg_2Si alloys modified with 0, 0.2 and 0.5 wt.% Li-Sb (the values following + signs were the upper limits while the value following – signs were the lower limits of the error bar).

Materials	YS/MPa	UCS/MPa	Uniform Elongation/%	Hardness/Hv
Al-20Mg_2Si	$111.7^{+2.6}_{-2.5}$	283^{+8}_{-10}	$12.8^{+1.0}_{-0.7}$	$90.8^{+2.0}_{-2.8}$
Al-20Mg2Si-0.2(Li-Sb)	$121.7^{+4.8}_{-3.1}$	306^{+5}_{-6}	$12.1^{+0.5}_{-0.6}$	$100.4^{+2.5}_{-3.1}$
Al-20Mg2Si-0.5(Li-Sb)	$178.8^{+3.1}_{-5.2}$	341^{+9}_{-7}	$12.3^{+1.3}_{-1.5}$	$103.8^{+1.1}_{-1.5}$

However, it is worth to noting that with Li-Sb content increasing from 0.2 to 0.5 wt.%, similar microstructure features were observed and the size of primary Mg_2Si still kept within the range of ~15–25 μm (Figure 2b,c), while the UCS increases significantly (from 306 to 341 MPa). Moreover,

except Al and Mg_2Si, no other phases that are beneficial to the mechanical properties of the alloy were detected (Figure 1a–c). Therefore, other factors, like the morphology of primary Mg_2Si, may also influence mechanical properties of the Al-20Mg_2Si alloy.

Typical 3-D morphologies of primary Mg_2Si in Al-20Mg_2Si alloys without and with various Li-Sb additions are given in Figure 7a–d. As we can see, with the content of Li and Sb increasing from 0 to 0.2 and then to 0.5 wt.%, the morphology of primary Mg_2Si transformed from coarse dendrite (Figure 7a) to coexistence of defective truncated octahedron and perfect truncated octahedron (Figure 7b–c) and finally to a perfect truncated octahedral shape (Figure 7d). According to the literature, defective truncated octahedron can separate the α-Al matrix in the growth defect to some extent [3], leading to lower UCS of the alloy modified with 0.2 wt.% Li-Sb as compared to the alloy modified with 0.5 wt.% Li-Sb (Table 1). In addition, with the content of Li-Sb increasing from 0.2 to 0.5 wt.%, the size of eutectic Mg_2Si decreased slightly (Figure 7e–g), which agrees well with the OM observations (Figure 2d–f). The refined size of eutectic phase is propitious to the improvement in the microhardness in modified alloys. Unfortunately, because Mg_2Si particles are brittle, their existence is harmful to the plasticity of Al-20Mg_2Si alloy [5,27]. Thus, controlling the morphology and size of primary Mg_2Si has little effect on improving plasticity of the modified Al-20Mg_2Si alloy.

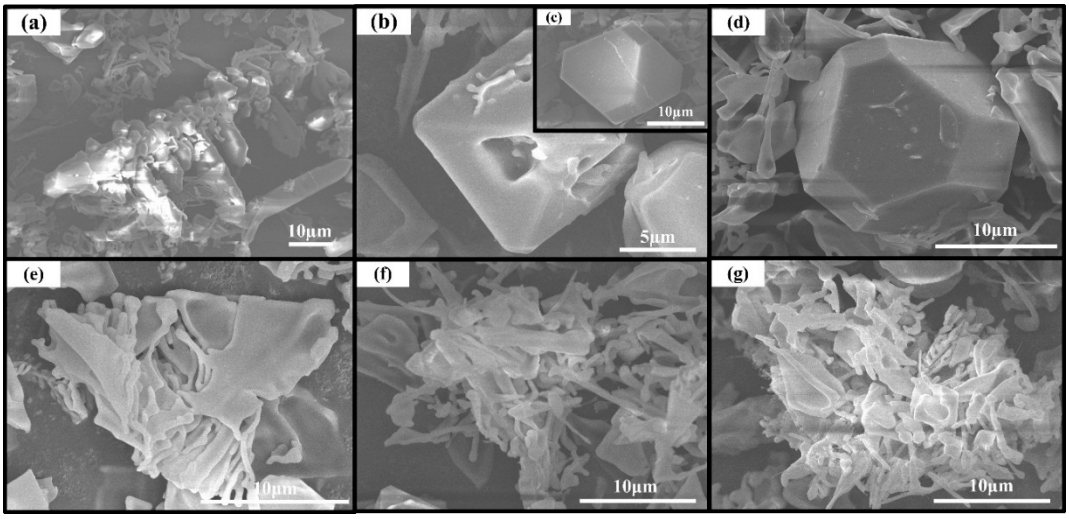

Figure 7. FESEM images of primary and eutectic Mg_2Si extracted from Al–20Mg_2Si alloys without and with various Li and Sb additions: primary Mg_2Si in (**a**) 0; (**b**)–(**c**) 0.2; (**d**) 0.5 wt.% Li-Sb; and eutectic Mg_2Si in (**e**) 0; (**f**) 0.2; and (**g**) 0.5 wt.% Li-Sb.

4. Conclusions

In this paper, the effect of Li_2Sb nucleus on microstructure and mechanical properties of Al-20Mg_2Si alloys was investigated and the main conclusions are drawn as following:

(1) The 3-D morphology of primary Mg_2Si was observed by extracting the Mg_2Si crystals from Al–20Mg_2Si alloys. With the addition of Li-Sb, the size of primary Mg_2Si decreased from ~300 to ~15–25 μm and the morphology changed from coarse dendrite to defective truncated octahedron and finally to perfect truncated octahedral shape.

(2) The modification mechanism of Li-Sb can be concluded as follows: Li_2Sb can act as better substrates to enhance the heterogeneous nucleation rate of primary Mg_2Si; meanwhile, excess Li atoms were absorbed on and restricted the growth of {100} facets. The modification effect of Li-Sb was better than that of either Li or Sb, respectively.

(3) Influence of Li_2Sb on mechanical properties of Al–20Mg_2Si alloys was also investigated. With the addition of Li and Sb, ultimate compression strength (UCS) of Al-20Mg_2Si alloys increased from ~283 to ~341 MPa and the yield strength (YS) at 0.2% offset increased from ~112 to ~179 MPa,

while almost no change was seen in the uniform elongation. The addition of Li and Sb also led to the increase in microhardness of α-Al matrix from ~91 to ~104 Hv.

Acknowledgments: Financial supports from The Natural Science Foundation of China (Nos. 51474111 and 51501069) and The Research Project of Science and Technology of Department of Education of Jilin Province (2015–482) are greatly acknowledged. Partial financial supports come from The Youth Scientific Research Fund Project of Jilin Province (No. 20160520120JH), The Fundamental Research Funds for the Central Universities (JCKY-QKJC02) and The ChangBai Mountain Scholars Program (2013014).

Author Contributions: Hong-Chen Yu and Hui-Yuan Wang conceived and designed the experiments; Hong-Chen Yu and Chao Li performed the experiments; Hong-Chen Yu, Hui-Yuan Wang, Lei Chen, Min Zha, Cheng Wang and Qi-Chuan Jiang analyzed the data; Hui-Yuan Wang, Min Zha and Cheng Wang contributed reagents/materials/analysis tools; Hong-Chen Yu wrote the paper.

Conflicts of Interest: The authors declare no conflict of interest.

References

1. Du, Q.; Li, Y.J. An extension of the Kampmann-Wagner numerical model towards as-cast grain size prediction of multicomponent aluminum alloys. *Acta Mater.* **2014**, *71*, 380–389. [CrossRef]
2. Kim, Y.M.; Wang, L.; You, B.S. Grain refinement of Mg-Al cast alloy by the addition of manganese carbonate. *J. Alloys Compd.* **2010**, *490*, 695–699. [CrossRef]
3. Li, C.; Liu, X.F.; Wu, Y.Y. Refinement and modification performance of Al-P master alloy on primary Mg_2Si in Al–Mg–Si alloys. *J. Alloys. Compd.* **2008**, *465*, 145–150. [CrossRef]
4. VaziriYeganeh, S.E.; Razaghian, A.; Emamy, M. The influence of Cu-15P master alloy on the microstructure and tensile properties of Al-25 wt% Mg_2Si composite before and after hot-extrusion. *Mater. Sci. Eng. A* **2013**, *566*, 1–7.
5. Emamy, M.; Khorshidi, R.; Raouf, A.H. The influence of pure Na on the microstructure and tensile properties of Al-Mg_2Si metal matrix composite. *Mater. Sci. Eng. A* **2011**, *528*, 4337–4342. [CrossRef]
6. Li, C.; Wu, Y.Y.; Li, H.; Liu, X.F. Morphological evolution and growth mechanism of primary Mg_2Si phase in Al–Mg_2Si alloys. *Acta Mater.* **2011**, *59*, 1058–1067. [CrossRef]
7. Mabuchi, M.; Higashj, K. Strengthening mechanisms of Mg-Si alloys. *Acta Mater.* **1996**, *44*, 4611–4618. [CrossRef]
8. Wang, L.; Qin, X.Y. The effect of mechanical milling on the formation of nanocrystalline Mg_2Si through solid-state reaction. *Scr. Mater.* **2003**, *49*, 243–248. [CrossRef]
9. Ardakan, A.H.; Ajersch, F. Thermodynamic evaluation of hypereutectic Al-Si (A390) alloy with addition of Mg. *Acta Mater.* **2010**, *58*, 3422–3428. [CrossRef]
10. Qin, Q.D.; Li, W.X.; Zhao, K.W.; Qiu, S.L.; Zhao, Y.G. Effect of modification and aging treatment on mechanical properties of Mg_2Si/Al composite. *Mater. Sci. Eng. A* **2010**, *527*, 2253–2257. [CrossRef]
11. Nasiri, N.; Emamy, M.; Malekan, A.; Norouzi, M.H. Microstructure and tensile properties of cast Al-15%Mg_2Si composite: Effects of phosphorous addition and heat treatment. *Mater. Sci. Eng. A* **2012**, *556*, 446–453. [CrossRef]
12. Khorshidi, R.; Hassani, A.; Rauof, A.H.; Emamy, M. Selection of an optimal refinement condition to achieve maximum tensile properties of Al-15%Mg_2Si composite based on TOPSIS method. *Mater. Des.* **2013**, *46*, 442–450. [CrossRef]
13. Soltani, N.; Jafari Nodooshan, H.R.; Bahrami, A.; Pech Canul, M.I.; Liu, W.C.; Wu, G.H. Effect of hot extrusion on wear properties of Al-15 wt.% Mg_2Si *in situ* metal matrix composites. *Mater. Des.* **2014**, *53*, 774–781. [CrossRef]
14. Zhang, J.; Fan, Z.; Wang, Y.Q.; Zhou, B.L. Equilibrium pseudobinary Al-Mg_2Si phase diagram. *Mater. Sci. Technol.* **2001**, *17*, 494–496. [CrossRef]
15. Jiang, Q.C.; Wang, H.Y.; Wang, Y.; Ma, B.X.; Wang, J.G. Modification of Mg_2Si in Mg-Si alloys with yttrium. *Mater. Sci. Eng. A* **2005**, *392*, 130–135. [CrossRef]
16. Emamy, M.; Emami, A.R.; Tavighi, K. The effect of Cu addition and solution heat treatment on the microstructure, hardness and tensile properties of Al-15%Mg_2Si-0.15%Li composite. *Mater. Sci. Eng. A* **2013**, *576*, 36–44. [CrossRef]

17. Chen, L.; Wang, H.Y.; Li, Y.J.; Zha, M.; Jiang, Q.C. Morphology and size control of octahedral and cubic primary Mg_2Si in an Mg-Si system by regulating Sr contents. *Cryst. Eng. Comm.* **2014**, *16*, 448–454. [CrossRef]
18. Hou, J.; Li, C.; Liu, X.F. Nucleating role of an effective *in situ* Mg_3P_2 on Mg_2Si in Mg-Al-Si alloys. *J. Alloys Compd.* **2011**, *509*, 735–739. [CrossRef]
19. Yuan, G.Y.; Liu, Z.L.; Wang, Q.D.; Ding, W.J. Microstructure refinement of Mg-Al-Zn-Si alloys. *Mater. Lett.* **2002**, *56*, 53–58. [CrossRef]
20. Chen, L.; Wang, H.Y.; Luo, D.; Zhang, H.Y.; Liu, B.; Jiang, Q.C. Synthesis of octahedron and truncated octahedron primary Mg_2Si by controlling the Sb contents. *Cryst. Eng. Comm.* **2013**, *15*, 1787–1793. [CrossRef]
21. Alizadeh, R.; Mahmudi, R. Effects of Sb addition on the modification of Mg_2Si particles and high-temperature mechanical properties of cast Mg-4Zn-2Si alloy. *J. Alloys Compd.* **2011**, *509*, 9195–9199. [CrossRef]
22. Wang, H.Y.; Li, Q.; Liu, B.; Zhang, N.; Chen, L.; Wang, J.G.; Jiang, Q.C. Modification of primary Mg_2Si in Mg-4Si alloys with antimony. *Metall. Mater. Trans. A* **2012**, *43*, 4926–4932. [CrossRef]
23. *Powder Diffraction File Card Nos. 26–0651 (Li_2Sb) and (Mg_2Si (65–2988) (CD ROM)*; International Center for Diffraction Data (ICDD): Newtown Square, PA, USA.
24. Khorshidia, R.; Raoufa, A.H.; Emamy, M.; Campbell, J. The study of Li effect on the microstructure and tensile properties of cast Al-Mg_2Si metal matrix composite. *J. Alloys Compd.* **2011**, *509*, 9026–9033. [CrossRef]
25. Yu, H.C.; Wang, H.Y.; Chen, L.; Liu, F.; Wang, C.; Jiang, Q.C. Heterogeneous nucleation of Mg_2Si on $CaSb_2$ nucleus in Al–Mg–Si alloys. *Cryst. Eng. Comm.* **2015**, *17*, 7048–7055. [CrossRef]
26. Nie, J.F.; Wu, Y.Y.; Li, P.T.; Li, H.; Liu, X.F. Morphological evolution of TiC from octahedron to cube induced by elemental nickel. *Cryst. Eng. Comm.* **2012**, *14*, 2213–2221. [CrossRef]
27. Azarbarmas, M.; Emamy, M.; Rassizadehghani, J.; Alipour, M.; Karamouz, M. The influence of beryllium addition on the microstructure and mechanical properties of Al-15%Mg_2Si in-situ metal matrix composite. *Mater. Sci. Eng. A* **2011**, *528*, 8205–8211. [CrossRef]